



# CHORUS

This is the accepted manuscript made available via CHORUS. The article has been published as:

## Polarization-Dependent Interference of Coherent Scattering from Orthogonal Dipole Moments of a Resonantly Excited Quantum Dot

Disheng Chen, Gary R. Lander, Glenn S. Solomon, and Edward B. Flagg

Phys. Rev. Lett. **118**, 037401 — Published 20 January 2017

DOI: [10.1103/PhysRevLett.118.037401](https://doi.org/10.1103/PhysRevLett.118.037401)

# Polarization-dependent interference of coherent scattering from orthogonal dipole moments of a resonantly excited quantum dot

Disheng Chen,<sup>1</sup> Gary R. Lander,<sup>1</sup> Glenn S. Solomon,<sup>2</sup> and Edward B. Flagg<sup>1,\*</sup>

<sup>1</sup>*Department of Physics and Astronomy, West Virginia University, Morgantown, WV 26506, USA*

<sup>2</sup>*Joint Quantum Institute, National Institute of Standards and Technology,*

*& University of Maryland, Gaithersburg, MD, USA.*

(Dated: December 27, 2016)

Resonant photoluminescence excitation (RPLE) spectra of a neutral InGaAs quantum dot show unconventional line-shapes that depend on the detection polarization. We characterize this phenomenon by performing polarization-dependent RPLE measurements and simulating the measured spectra with a 3-level quantum model. The spectra are explained by interference between fields coherently scattered from the two fine structure split exciton states, and the measurements enable extraction of the steady-state coherence between the two exciton states.

Light-matter interactions in semiconductor nanostructures have attracted significant research interest because of both fundamental physics questions and practical concerns. Epitaxially grown quantum dots (QDs), with their narrow emission linewidths and atom-like density of states in a solid state system, are archetypical elements of study and are potentially useful for many reasons. For example, they have been demonstrated to be efficient sources for single photons [1, 2] and entangled photon pairs [3, 4], both of which are capabilities applicable to quantum information science. Resonant continuous wave (CW) excitation of the bound exciton states has allowed measurement of a number of phenomena that cannot be seen with either incoherent or pulsed excitation. Some examples are the Mollow triplet emission from dressed states of a 2-level quantum system [5–7], and the related Mollow quintuplet from dressed states of a V-system [8]. The selectivity and precision of resonant excitation have also allowed the production of high-distinguishability photons [9, 10], and measurement of charge and spin fluctuations in the local solid state environment [11–13]. Many resonant excitation experiments use crossed polarizers to attenuate the laser scattering and allow detection of the resonance fluorescence [10–12, 14–16]. In such a case, the fluorescence detection is necessarily polarization-selective. Here we show that when polarization-selective detection is used, orthogonal dipole moments, such as those of a neutral QD or those of a charged QD in a transverse magnetic field, cause an interference effect that results in an unconventionally shaped excitation spectrum.

In typical epitaxially grown quantum dots, the anisotropic exchange interaction results in two bound exciton states split by several  $\mu\text{eV}$  with orthogonal transition dipole moments that emit linearly polarized fluorescence [17–20]. When the fine structure splitting is on the order of the transition linewidth, a CW excitation laser can interact with both exciton states simultaneously if it is polarized so as to have a non-zero projection onto both dipole moments. The QD-field interaction will cause

both coherent scattering at the laser frequency [5, 21, 22] and incoherent spontaneous emission at the transition dipole frequencies. The fields coherently scattered from the two non-degenerate orthogonal dipoles will be at the same frequency but phase-shifted relative to each other. Interference between these fields results in a noticeable difference between the shapes of the excitation spectra for detection polarizations parallel and orthogonal to the excitation. This phenomenon is not present in pulsed excitation experiments, where the emission is generally unpolarized when both dipole moments are excited [23]. By measuring polarization-dependent excitation spectra for polarizations both aligned to the transition dipole moments and 45-degrees rotated relative to them, we can extract the real part of the coherence between the two fine structure states induced by the excitation.

The sample studied in this work consists of self-assembled InGaAs QDs embedded in a  $4\text{-}\lambda$  GaAs waveguide bounded by two AlGaAs/GaAs distributed Bragg reflectors (DBRs), which form a planar microcavity. The

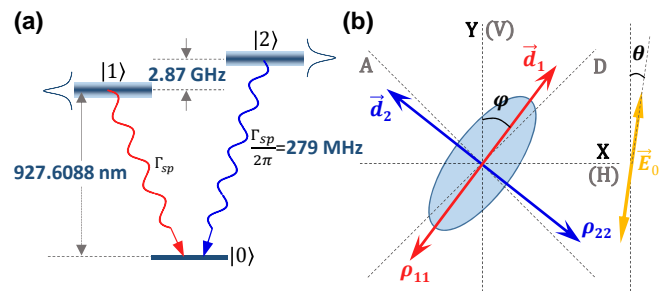


FIG. 1. (a) Quantum dot energy diagram. The population spontaneous decay rate is determined to be  $\Gamma_{sp}/2\pi = (279.2 \pm 0.9)$  MHz by time-resolved fluorescence measurements (see Supplementary Material [24]), and the fine structure splitting is  $\Delta_{FSS}/2\pi = (2.869 \pm 0.001)$  GHz. (b) Polarization and electric dipole moment orientations. The lower energy  $\mathbf{d}_1$  and higher energy  $\mathbf{d}_2$  dipole moments are shown, as is the polarization of the excitation field,  $\mathbf{E}_0$ . The shape of the QD is shown schematically with its asymmetry exaggerated.

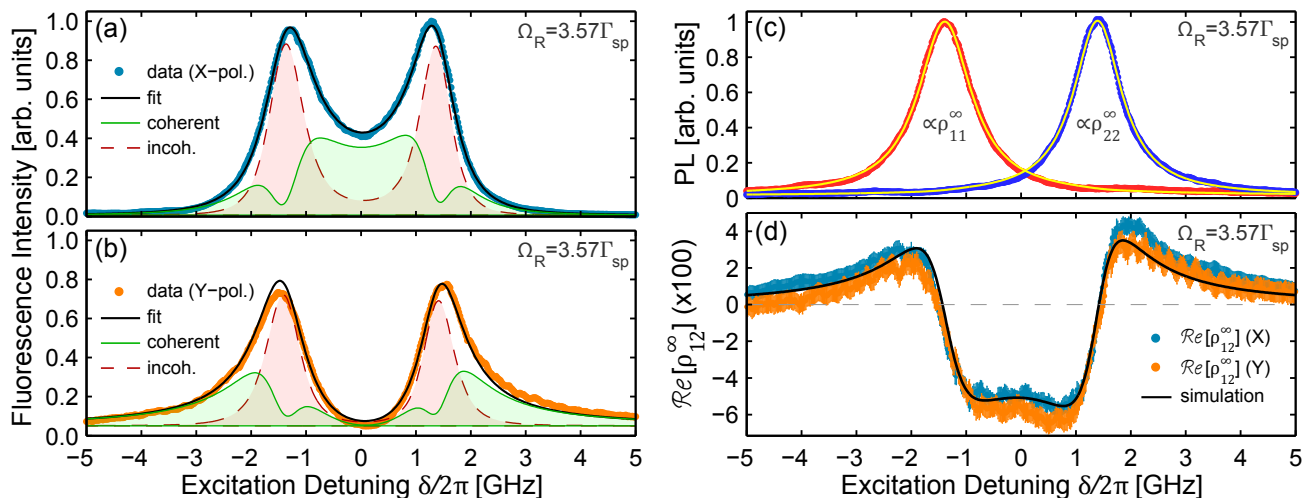


FIG. 2. Example RPLE spectra recorded with  $\Omega_R = 3.57\Gamma_{sp}$  and detection polarization chosen to be (a) X (blue points), (b) Y (orange points), or (c) to eliminate either the low-energy or high-energy peak. The black solid lines in (a) and (b) are fittings following Eqns. 1 and 2. The green (solid) and red (dashed) lines underneath the spectra are the calculated portions of coherent and incoherent scattering, respectively. The two yellow curves in (c) are the fittings obtained by using the calculated exciton populations  $\rho_{11}^{\infty}$  and  $\rho_{22}^{\infty}$  from the 3-level model. (d) The coherence  $\text{Re}[\rho_{12}^{\infty}]$  extracted from the curves in (a) and (b); the colors indicate the polarization whence the coherence was extracted. The black solid curve in (d) is not a fit but the calculation of  $\text{Re}[\rho_{12}^{\infty}]$  using the same parameters found in the previous fittings in (a) and (b).

sample is maintained at 4.2 K in a closed-cycle cryostat. The energy level structure of a neutral QD is depicted in Fig. 1(a), and the associated dipole moment orientations are shown in Fig. 1(b). The system is investigated using polarization-dependent resonant photoluminescence excitation (RPLE) spectroscopy, which measures the total fluorescence from the QD as the frequency of the CW excitation laser is scanned across the QD resonance. Multiple RPLE spectra are recorded using different detection polarizations under the same excitation polarization. Rather than using crossed polarizers to discriminate between fluorescence and laser scattering [14, 15], we instead use modal discrimination between the waveguide mode and the Fabry-Perot mode of the planar microcavity [6–8, 13]. A resonant laser with a 1 MHz linewidth is coupled into the waveguide mode through the cleaved edge of the sample. The photoluminescence (PL) is coupled out through the Fabry-Perot mode normal to the sample plane. It is first collimated by an aspheric objective lens with NA=0.5, and then guided through a pair of liquid crystal variable retarders (LCVRs) and a linear polarizer. The light then enters a monochromator to select the PL from just one QD, which is detected by a thermoelectrically cooled CCD camera and spectrally integrated. The fast axes of the two LCVRs are aligned to the vertical and diagonal directions, allowing us to rotate any polarization state onto the measurement axis determined by the linear polarizer. Therefore, we can fully characterize the polarization state of the PL via the Stokes vector by measuring the intensity projection on the horizontal (X), vertical (Y), diagonal (D), anti-

diagonal (A), left-circular (L), and right-circular (R) polarizations.

Figures 2(a-b) show two normalized RPLE spectra under the same excitation conditions but with different detection polarizations: horizontal (X) or vertical (Y). Neither spectrum can be reconstructed by incoherently adding two Lorentzian lines centered at the two peaks as would be the case if the fluorescence consisted solely of spontaneous emission. This implies that to account for the observed unconventional line shapes, we must also include a polarization-dependent interference occurring between photons coherently scattered by the two fine structure states. Clear evidence of the presence of such interference can be seen at zero detuning, where a  $90^\circ$  polarization switching with respect to the excitation field is present, i.e., the scattered light becomes highly X-polarized even though the excitation is Y-polarized.

An analysis of the proportions of coherent and incoherent scattering in these spectra illustrates the underlying physics. In Figs. 2(a-b), these calculated proportions are denoted by the green (solid) and red (dashed) lines for coherent and incoherent scattering, respectively. As expected, the incoherent scattering looks much like the incoherent sum of two Lorentzians; the small overlap of the two peaks leads to a negligible contribution at zero detuning. In contrast, because the coherent scattering is always at the laser wavelength, a pronounced interference effect is expected between contributions from the two dipoles. The relative phase shift of the coherently scattered photons is determined by the detuning of the laser with respect to each transition energy. This is sim-

ilar to a driven harmonic oscillator: red-detuned driving results in a negative (lagging) phase while blue-detuned driving leads to a positive (leading) phase. Thus at zero detuning, the fields coherently scattered from the two dipoles have a relative phase shift even though the field polarizations are still aligned to each dipole. The detection polarization determines whether these phase-shifted fields combine constructively (for horizontal (X) polarization) or destructively (for vertical (Y) polarization). This explains the observed enhancement or diminution of the PL signal around zero detuning in Figs. 2(a-b), respectively.

In contrast to the excitation spectrum presented in Figs. 2(a-b), the emission spectrum for a resonantly excited QD should be a Mollow quintuplet [8]. In the emission spectrum, the coherent scattering would appear as a delta function at the laser frequency, while the incoherent scattering from the dressed states [5, 25] appears at the laser frequency and at four peaks beside it. Here the spectrometer resolution was not high enough to resolve the separate peaks, so the fluorescence was spectrally integrated and the excitation spectrum analyzed. In future work, the coherent portion of the fluorescence could be measured separately from the incoherent part via heterodyne measurements [22] and compared to the theoretical models in Figs. 2(a-b).

We model the neutral QD as a 3-level V-system and calculate its density matrix using a quantum master equation in Lindblad form [26, 27]; we treat the excitation interaction semi-classically under the rotating wave approximation [26, 28]. The scattered field, both coherent and incoherent parts, can be linked to elements of the density matrix [26, 29]. The final expressions for the X- and Y-polarized, and total RPLE intensities are as follows (see Supplementary Material [24] for the detailed derivation):

$$I_X = I_0 \{ \sin^2(\varphi) \rho_{11}^\infty + \cos^2(\varphi) \rho_{22}^\infty - \sin(2\varphi) \mathcal{R}e[\rho_{12}^\infty] \} \quad (1)$$

$$I_Y = I_0 \{ \cos^2(\varphi) \rho_{11}^\infty + \sin^2(\varphi) \rho_{22}^\infty + \sin(2\varphi) \mathcal{R}e[\rho_{12}^\infty] \} \quad (2)$$

$$I = I_X + I_Y = I_0 \{ \rho_{11}^\infty + \rho_{22}^\infty \} \quad (3)$$

where  $\rho_{11}^\infty$  and  $\rho_{22}^\infty$  are the populations in levels  $|1\rangle$  and  $|2\rangle$ ,  $\rho_{12}^\infty$  is the coherence between the two excited states, the superscript  $\infty$  represents the steady-state solutions, and  $\varphi$  is the angle of the dipole moment  $\mathbf{d}_1$  with respect to the Y-axis (see Fig. 1(b)).  $I_0$  is the intensity constant,  $I_0 = \omega_0^4 d^2 / 128 \pi^4 \epsilon_0 c^3 r^2$ , where  $d \approx |\mathbf{d}_1| \approx |\mathbf{d}_2|$  is the magnitude of the transition dipole moment,  $\omega_0 = (\omega_1 + \omega_2)/2$  is the average transition frequency, and  $r$  is the distance from the QD to the detector. In this work, we label all the resonant excitation powers with the corresponding overall Rabi frequency  $\Omega_R = d|\mathbf{E}_0|/\hbar$  in units of the population decay rate  $\Gamma_{sp}$ . The individual Rabi frequency  $\Omega_j$  for level  $|j\rangle$  is  $\Omega_R \cos(\beta_j)$  where  $\beta_j$  is the angle between the electric dipole moment  $\mathbf{d}_j$  and the excitation field  $\mathbf{E}_0$ .

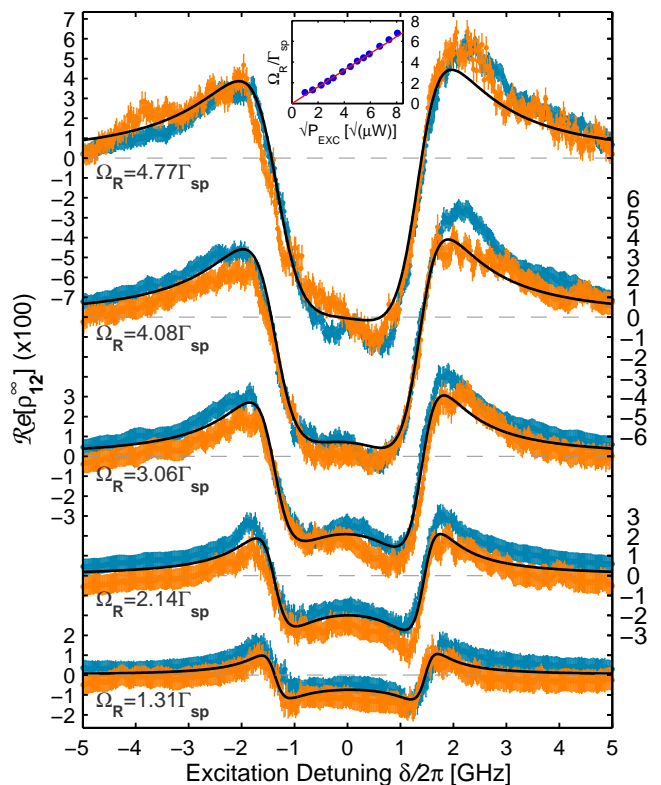


FIG. 3.  $\mathcal{R}e[\rho_{12}^\infty]$  extracted at different excitation powers. The curves are vertically offset for clarity. The color scheme used in each pair is the same as Fig. 2(d), i.e., orange is extracted from the Y-polarized RPLE and blue from X-polarized. The black solid curves are the calculation of  $\mathcal{R}e[\rho_{12}^\infty]$  at different Rabi frequencies  $\Omega_R$  determined by fittings to the raw RPLE data similar to Figs. 2(a-b). The other model parameters are the same throughout all the calculations. Inset: Rabi frequency  $\Omega_R$  vs. the square root of the excitation power. The red straight line is a linear fit with a slope of  $(0.806 \pm 0.011)\Gamma_{sp}/\sqrt{\mu W}$ .

The RPLE intensities in Eqns. 1 & 2 are not just proportional to the excited state populations  $\rho_{11}^\infty$  and  $\rho_{22}^\infty$ , which would be the case for a 2-level system. Instead, they are modified by the real part of the coherence between the two excited states, i.e.,  $\mathcal{R}e[\rho_{12}^\infty]$ . In contrast, the total PL intensity in Eqn. 3 is still proportional to the total population in both excited states. The difference in the sign of the third terms in  $I_X$  and  $I_Y$  explains the difference between the X-polarized and Y-polarized RPLE spectra. By simultaneously fitting Eqns. 1 and 2 to multiple sets of RPLE spectra measured at different excitation powers, we determine the orientation of the dipole moment  $\mathbf{d}_1$  to be  $\varphi = 44.74^\circ \pm 0.04^\circ$  with respect to the Y-axis, and the direction of the resonant excitation field  $\mathbf{E}_0$  to be  $\theta = 3.37^\circ \pm 0.07^\circ$  with respect to the Y-axis. Thus the electric dipole moments of the QD,  $\mathbf{d}_1$  and  $\mathbf{d}_2$ , are almost aligned to the diagonal (D) and the anti-diagonal (A) directions, respectively, which is consistent with our Stokes parameter measurement and

analysis of the PL (see Supplementary Material [24]).  $\mathbf{E}_0$  is nominally aligned to the Y-axis because the excitation laser is propagating in the X-direction along the waveguide mode. But  $\mathbf{E}_0$  may deviate from that alignment due to unintentional non-normal incidence of the laser on the air-GaAs interface, which would cause refraction of the beam away from the X-direction.

Figure 2(c) shows the RPLE spectra measured with the LCVRs tuned to block the PL emitted from either the high-energy or low-energy state of the fine structure doublet. Since that approach measures the emission from only one energy level at a time, there is no interference effect in these spectra. Each spectrum can be directly fitted with the corresponding excited population as  $I_1 = A_1\rho_{11}^\infty + B_1$  and  $I_2 = A_2\rho_{22}^\infty + B_2$  for states  $|1\rangle$  and  $|2\rangle$ , respectively, where  $A_j$  and  $B_j$  are fitting parameters. To account for the polarization-dependent absorption of the optics in the detection path, we use the fact that both the sum of the spectra in Figs. 2(a-b) and the sum of the spectra in Fig. 2(c) are proportional to the total excited population in the QD (See Supplementary Material [24]). This ensures accurate extraction of the real part of the coherence  $\text{Re}[\rho_{12}^\infty]$  as shown in Fig. 2(d). Using parameters from the fits in Figs. 2(a-b), the 3-level V-system simulation reproduces the shape of the coherence successfully (black curve in Fig. 2(d)).

Figure 3 shows the extracted real part of the coherence for multiple excitation powers. As the excitation power increases, the dispersive line shapes centered at each fine structure resonance increase in magnitude and experience power broadening as is expected for coherent excitation [28]. Again, the simulations match the data well and even reproduce the slight asymmetry about zero detuning. We note that to obtain an observable asymmetry requires two conditions: (1) the dipole moments of the QD must not be oriented 45 degrees with respect to the excitation field, and (2) the excitation power must be high. The single condition of tilted QD dipole moments is not enough to achieve this asymmetry according to the simulations (see Supplementary Material [24]), implying that this is a non-linear effect happening at high excitation power. In the inset of Fig. 3, the Rabi frequencies extracted from the fittings follow a linear relationship with respect to the square root of power, as expected.

There are several differences between the CW excitation used in this study and experiments that use pulsed excitation to create and measure coherence (e.g. ref. [23]). Under pulsed excitation, a coherent superposition of two excited states is created by the excitation pulse, which then evolves freely over time and experiences quantum beats at a frequency determined by the fine structure splitting  $\Delta_{FSS}$ . Since  $\Delta_{FSS} \gg \Gamma_{sp}$ , it most often leads to a vanishingly small polarization in the time-integrated fluorescence. In addition, the fluorescence is entirely spontaneous emission, which is incoherent; there is no coherent scattering. In contrast, under CW excita-

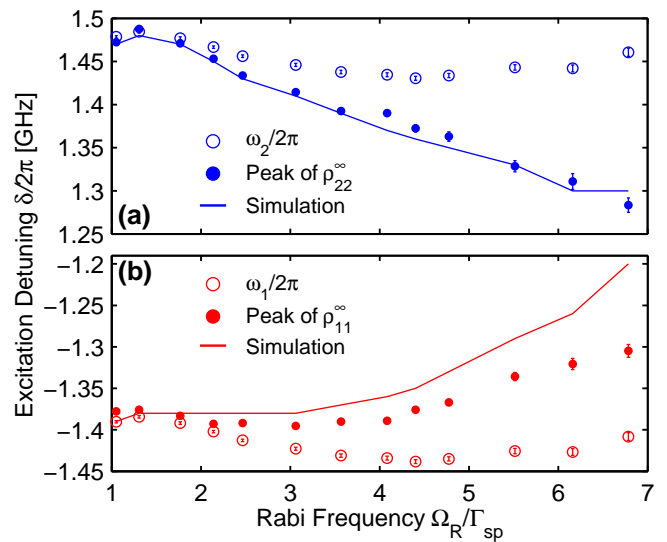


FIG. 4. (a) The evolution of the high-energy state's intrinsic resonance frequency  $\omega_2/2\pi$  (blue open circles) and the evolution of the peak positions of the excited population  $\rho_{22}^\infty$  obtained by either a Lorentzian fitting (blue dots) or the V-system simulation (blue line). (b) The evolution of the low-energy state's intrinsic resonance frequency  $\omega_1/2\pi$  (red open circles) and the evolution of the peak positions of the excited population  $\rho_{11}^\infty$  obtained by either a Lorentzian fitting (red dots) or the V-system simulation (red line).

tion coherent scattering occurs and a strong polarization results. Moreover, the density matrix under CW excitation is in a steady-state that depends on the excitation power and detuning, rather than a time-varying state.

The solid dots in Figs. 4(a-b) are the peak positions of the spectra in Fig. 2(c) obtained by fitting them each with a Lorentzian function (Fig. S3 in Supplementary Material [24]). We find that the two resonance peaks move towards each other as the power increases; this is due to the AC Stark effect. For example, when the laser is near resonance with the low-energy state  $|1\rangle$ , the excitation field is red-detuned with respect to the high-energy state  $|2\rangle$ . This detuning pushes state  $|0\rangle$  and state  $|2\rangle$  away from each other via the AC Stark effect [30–32]. The red-shift of the ground state in turn effectively increases the transition energy of state  $|1\rangle$ . Since the AC Stark effect gets stronger at higher excitation power, the low-energy state  $|1\rangle$  moves continuously towards the higher energy side of the spectrum. Similarly, the high-energy state  $|2\rangle$  experiences a red-shift in its transition energy as the power increases. We calculate the expected resonance positions based on the fitting parameters found in Fig. 2(a) and depicted them as solid lines in Figs. 4(a-b). They are in good agreement with the data, especially for the high-energy state.

The open circles in Figs. 4(a-b) represent the fitting parameters  $\omega_2/2\pi$  and  $\omega_1/2\pi$ , called the intrinsic transition frequencies for states  $|2\rangle$  and  $|1\rangle$ . These parameters are

determined by the intrinsic properties of the QD, which should not change if the QD's local environment is not disturbed. Therefore, the variation of  $\omega_2/2\pi$  and  $\omega_1/2\pi$  shown in Figs. 4(a-b) reflects the fluctuations of the local environment caused by the resonant excitation laser [13]. Further discussion on these fluctuations is given in Section 6 of the Supplementary Material [24].

In this letter, we have demonstrated and modeled an interference effect that occurs during CW resonant excitation of a multi-level quantum system. Including coherent scattering is necessary to explain the strong polarization difference between the excitation and the emission. Such a phenomenon does not occur under incoherent or pulsed excitation. Comparison of spectra with different detection polarizations allows extraction of the steady-state coherence generated between the two excited states. All the spectra and coherences are correctly reproduced by a density matrix model of the QD. Similar effects must be accounted for in any situation where there are two non-degenerate orthogonal transition dipole moments and only a certain polarization is detected. One example is the “dark-field” resonant excitation and detection technique [15] in combination with a charged QD in an in-plane magnetic field.

We would like to acknowledge Tim Thomay for helpful discussions. This work was supported by the National Science Foundation (DMR-1452840).

---

\* edward.flagg@mail.wvu.edu

- [1] P. Michler, A. Kiraz, C. Becher, W. V. Schoenfeld, P. M. Petroff, L. Zhang, E. Hu, and A. Imamoglu, *Science* **290**, 2282 (2000).
- [2] C. Santori, M. Pelton, G. Solomon, Y. Dale, and Y. Yamamoto, *Physical Review Letters* **86**, 1502 (2001).
- [3] N. Akopian, N. H. Lindner, E. Poem, Y. Berlatzky, J. Avron, D. Gershoni, B. D. Gerardot, and P. M. Petroff, *Physical Review Letters* **96**, 130501 (2006).
- [4] R. Trotta, J. S. Wildmann, E. Zallo, O. G. Schmidt, and A. Rastelli, *Nano Letters* **14**, 3439 (2014).
- [5] B. R. Mollow, *Physical Review* **188**, 1969 (1969).
- [6] A. Muller, E. B. Flagg, P. Bianucci, X. Y. Wang, D. G. Deppe, W. Ma, J. Zhang, G. J. Salamo, M. Xiao, and C. K. Shih, *Physical Review Letters* **99**, 187402 (2007).
- [7] E. B. Flagg, A. Muller, J. W. Robertson, S. Founta, D. G. Deppe, M. Xiao, W. Ma, G. J. Salamo, and C. K. Shih, *Nature Physics* **5**, 203 (2009).
- [8] R.-C. Ge, S. Weiler, A. Ulhaq, S. M. Ulrich, M. Jetter, P. Michler, and S. Hughes, *Optics Letters* **38**, 1691 (2013).
- [9] Y.-M. He, Y. He, Y.-J. Wei, D. Wu, M. Atature, C. Schneider, S. Hffing, M. Kamp, C.-Y. Lu, and J.-W. Pan, *Nature Nanotechnology* **8**, 213 (2013).
- [10] A. V. Kuhlmann, J. H. Prechtel, J. Houel, A. Ludwig, D. Reuter, A. D. Wieck, and R. J. Warburton, *Nature Communications* **6**, 8204 (2015).
- [11] A. V. Kuhlmann, J. Houel, A. Ludwig, L. Greuter, D. Reuter, A. D. Wieck, M. Poggio, and R. J. Warburton, *Nature Physics* **9**, 570 (2013).
- [12] M. J. Stanley, C. Matthiesen, J. Hansom, C. Le Gall, C. H. H. Schulte, E. Clarke, and M. Atature, *Physical Review B* **90**, 195305 (2014).
- [13] D. Chen, G. R. Lander, K. S. Krowpman, G. S. Solomon, and E. B. Flagg, *Physical Review B* **93**, 115307 (2016).
- [14] N. A. Vamivakas, Y. Zhao, C.-Y. Lu, and M. Atature, *Nature Physics* **5**, 198 (2009).
- [15] A. V. Kuhlmann, J. Houel, D. Brunner, A. Ludwig, D. Reuter, A. D. Wieck, and R. J. Warburton, *Review of Scientific Instruments* **84**, 073905 (2013).
- [16] Y. He, Y.-M. He, J. Liu, Y.-J. Wei, H. Y. Ramirez, M. Atature, C. Schneider, M. Kamp, S. Hffing, C.-Y. Lu, and J.-W. Pan, *Physical Review Letters* **114**, 097402 (2015).
- [17] D. Gammon, E. S. Snow, B. V. Shanabrook, D. S. Katzer, and D. Park, *Physical Review Letters* **76**, 3005 (1996).
- [18] E. L. Ivchenko, *physica status solidi (a)* **164**, 487 (1997).
- [19] M. Bayer, G. Ortner, O. Stern, A. Kuther, A. A. Gorbunov, A. Forchel, P. Hawrylak, S. Fafard, K. Hinzer, T. L. Reinecke, S. N. Walck, J. P. Reithmaier, F. Klopff, and F. Schafer, *Physical Review B* **65**, 195315 (2002).
- [20] H. Tong and M. W. Wu, *Physical Review B* **83**, 235323 (2011).
- [21] F. Y. Wu, R. E. Grove, and S. Ezekiel, *Physical Review Letters* **35**, 1426 (1975).
- [22] M. Metcalfe, G. S. Solomon, and J. Lawall, *Applied Physics Letters* **102**, 231114 (2013).
- [23] N. H. Bonadeo, J. Erland, D. Gammon, D. Park, D. S. Katzer, and D. G. Steel, *Science* **282**, 1473 (1998).
- [24] See Supplementary Material, which includes Refs. [33-34].
- [25] C. Cohen-Tannoudji and S. Reynaud, *Journal of Physics B: Atomic and Molecular Physics* **10**, 345 (1977).
- [26] R. Loudon, *The Quantum Theory of Light* (OUP Oxford, 2000).
- [27] G. Lindblad, *Communications in Mathematical Physics* **48**, 119 (1976).
- [28] L. Allen and J. H. Eberly, *Optical Resonance and Two Level Atoms* (Wiley, New York, 1975).
- [29] M. O. Scully and M. S. Zubairy, *Quantum Optics* (Cambridge University Press, 1997).
- [30] T. Unold, K. Mueller, C. Lienau, T. Elsaesser, and A. D. Wieck, *Physical Review Letters* **92**, 157401 (2004).
- [31] A. Muller, W. Fang, J. Lawall, and G. S. Solomon, *Physical Review Letters* **101**, 027401 (2008).
- [32] A. Muller, W. Fang, J. Lawall, and G. S. Solomon, *Physical Review Letters* **103**, 217402 (2009).
- [33] H. S. Nguyen, G. Sallen, M. Abbarchi, R. Ferreira, C. Voisin, P. Roussignol, G. Cassabois, and C. Diederichs, *Physical Review B* **87**, 115305 (2013).
- [34] S.-Y. Lu and R. A. Chipman, *Journal of the Optical Society of America A* **13**, 1106 (1996).